Dalton Transactions

Cite this: *Dalton Trans.*, 2011, **40**, 5505

www.rsc.org/dalton

PAPER

Water-soluble alkylated bis{4′-(4-pyridyl)-2,2′:6′,2″-terpyridine}-ruthenium(II) complexes for use as photosensitizers in water oxidation: a complementary experimental and TD-DFT investigation†

Edwin C. Constable,*[a] Michael Devereux,[b] Emma L. Dunphy,[a] Catherine E. Housecroft,*[a] Jennifer A. Rudd[a] and Jennifer A. Zampese[a]

Received 7th December 2010, Accepted 14th March 2011
DOI: 10.1039/c0dt01714k

A series of *N*-alkylated derivatives $[RuL_2][PF_6]_4$ has been prepared from $[Ru(pytpy)_2][PF_6]_2$ (*N*-alkyl substituent = 4-cyanobenzyl, 4-nitrobenzyl, ethyl, cyanomethyl, allyl, octyl). Solution NMR spectroscopic, electrochemical and photophysical properties are reported, along with the single crystal structure of $[Ru(\mathbf{4})_2][PF_6]_4 \cdot H_2O$ (**4** = 4′-(4-(1-ethylpyridinio))-2,2′:6′,2′-terpyridine). Anion exchange leads to the water-soluble $[RuL_2][HSO_4]_4$ salts (*N*-alkyl substituent = benzyl, 4-cyanobenzyl, 4-nitrobenzyl, ethyl, cyanomethyl, allyl, octyl) and the NMR spectroscopic signatures of pairs of hexafluoridophosphate and hydrogensulfate salts are compared. The change in anion has little effect on the energies of absorptions in the electronic spectra, although for all complexes, decreases in extinction coefficients are observed. The emission spectra and lifetimes for the hexafluoridophosphate and hydrogensulfate salts show similar trends; all exhibit an emission close to 720–730 nm (λ_{ex} = 510 nm). For a given ligand, L, the emission lifetime decreases on going from $[RuL_2][PF_6]_4$ to $[RuL_2][HSO_4]_4$. However, trends are the same for both salts, *i.e.* the longest lived emitters are observed for *N*-ethyl, *N*-octyl and *N*-benzyl derivatives, and the shortest lived emitters are those containing cyano or nitro groups. Significantly, in the absorption spectra of the complexes, there is little variation in the energy of the MLCT band, suggesting that the character of the ligand orbital involved in the transition contains no character from the *N*-substituent. We have addressed this by carrying out a complementary DFT and TD-DFT study. Calculated absorption spectra predict a red shift in λ_{max} on going from $[Ru(pytpy)_2]^{2+}$ to $[RuL_2]^{4+}$, and little variation in λ_{max} within the series of $[RuL_2]^{4+}$ complexes; these results agree with experimental observations. Analysis of the compositions of the MOs involved in the MLCT transitions explain the experimental observations, showing that there is no contribution from orbitals on the *N*-alkyl substituents, consistent with the fact that the nature of the *N*-substituents has little influence on the energy of the MLCT band. The theoretical results also reveal satisfactory agreement between calculated and crystallographic data for $[Ru(\mathbf{1})_2]^{4+}$ (**1** = 4′-(4-(1-benzylpyridinio))-2,2′:6′,2′-terpyridine) and $[Ru(\mathbf{4})_2]^{4+}$.

Introduction

Complexes containing octahedral $\{M(tpy)_2\}$ cores (tpy = 2,2′:6′,2′-terpyridine) are ideal building blocks for the assembly of supramolecular architectures,[1–5] and units containing ruthenium(II) or osmium(II) are particularly advantageous. While being kinetically inert (low-spin d^6), the metal centres are redox active and the complexes exhibit photophysical properties that can be tuned by substituents, most readily introduced at the 4′-positions of the tpy ligands.[6] We have reported the effects of protonation and alkylation of the pyridine nitrogen atoms in $[ML_2][PF_6]_2$ (M = Fe or Ru; L = 4′-(2-pyridyl)-2,2′:6′,2′-terpyridine, 4′-(3-pyridyl)-2,2′:6′,2′-terpyridine or 4′-(4-pyridyl)-2,2′:6′,2′-terpyridine) on the absorption spectra and electrochemical properties of the complexes.[7–10] For alkylation of $[Fe(pytpy)_2][PF_6]_2$ (pytpy = 4′-(4-pyridyl)-2,2′:6′,2′-terpyridine), we have observed that a variety of alkyl (R = Me, $(CH_2)_9CH_3$, $(CH_2)_{15}CH_3$ CH_2Ph, $(CH_2)_3I$, $CH_2C{\equiv}CH$) groups result in a common red-shifting of the MLCT absorption causing an optical change from purple to blue. *N*-Alkylation is also responsible for a shift in the metal-centred reversible Fe^{2+}/Fe^{3+} process from +0.80 V in $[Fe(pytpy)_2][PF_6]_2$

[a]*Department of Chemistry, University of Basel, Spitalstrasse 51, CH-4056, Basel, Switzerland. E-mail: catherine.housecroft@unibas.ch, edwin.constable@unibas.ch; Fax: +41 61 267 1018; Tel: +41 61 267 1008*
[b]*Université Paris Descartes, Laboratoire de Chimie et Biochimie Pharmacologiques et Toxicologiques, UMR 8601 CNRS, UFR Biomedicale, 45 rue des Saints-Pères, 75270, Paris Cedex06, France*

† Electronic supplementary information (ESI) available: Ru basis set used in Gaussian 09; Figs. S1–S6. Comparable figures to Fig. 7 for $[RuL_2]^{4+}$ (L^+ = **1**–**3**, **5**–**7**). CCDC reference number 803992. For ESI and crystallographic data in CIF or other electronic format see DOI: 10.1039/c0dt01714k

to +0.82–0.89 V in $[Fe(N\text{-R-pytpy})_2][PF_6]_4$.[9] We have also demonstrated that with appropriate spacers in the organic *N*-substituents, $[M(N\text{-R-pytpy})_2]^{4+}$ complexes are flexible enough to function as motifs from which metallomacrocycles can be assembled.

In joint studies with Credi, we have applied the changes in luminescence brought about by the two-step *N*-protonation[11] of $[Ru(pytpy)_2]^{2+}$ or $[Os(pytpy)_2]^{2+}$ to the design of molecular switches and logic gates.[12,13] In addition to protonation and methylation,[8] our previous investigations of *N*-alkylations of $[Ru(pytpy)_2]^{2+}$ have focused mainly on substituents with pendant functionalities, *e.g.* CH_2CH_2OH, CH_2Br and tpy, as well as the derivative $[Ru(\mathbf{1})_2][PF_6]_4$.[14] More recently, in collaboration with Kaledin, Lian, Hill and Musaev, we have investigated the transfer of one electron from an MLCT excited state of $[Ru(4\text{-Mepytpy})_2]^{4+*}$ ($[4\text{-Mepytpy}]^+$ = 4′-(4-methylpyridinio)-2,2′:6′,2′-terpyridine) to $[S_2O_8]^{2-}$ in the first step of a three-component, homogenous water oxidation system.[15] We are, therefore, interested in investigating the extent to which altering the *N*-substituent, R, in $[4\text{-Rpytpy}]^+$ ligands can change the photophysical properties of the *N*-alkylated bis(4′-pyridyl-2,2′:6′,2′-terpyridinyl)ruthenium(II) complexes. For application of these complexes as photosensitizers in water oxidation, it is advantageous that they are water soluble. In this paper, we describe *N*-alkylation of the pendant pyridyl units in $[Ru(pytpy)_2][PF_6]_2$ to produce $[RuL_2][PF_6]_4$ in which L^+ = **2–7** (Scheme 1) and subsequent anion exchange to yield a series of water soluble $[RuL_2][HSO_4]_4$ complexes. We also present time-dependent density functional theory (TD-DFT) results for the $[RuL_2]^{4+}$ cations to assist in understanding the effects that changing the *N*-substituent has on the electronic absorption spectra of the complexes.

Experimental

^{1}H NMR spectra were recorded on a Bruker DRX-500 MHz NMR spectrometer; chemical shifts are referenced to residual solvent peaks with TMS = δ 0 ppm. ^{13}C NMR spectra recorded in D_2O were referenced to DSS added to the solution (see text). MALDI-TOF mass spectra were recorded on a PerSeptive Biosystems Voyager spectrometer. Electronic absorption and emission spectra were recorded using an Agilent 8453 spectrophotometer and Shimadzu RF-5301 PC spectrofluorometer, respectively. Lifetime measurements were made using a Mini-Tau spectrometer from Edinburgh Instruments (475 nm laser diode). TGA-MS measurements were carried out on a Mettler Toledo TGA/SDTA851^e with Pfeiffer Vacuum Thermostar™.

Electrochemical measurements were carried out using an Eco Chemie Autolab PGSTAT 20 system with glassy carbon working and platinum auxiliary electrodes; a silver wire was used as a pseudo-reference electrode. Solvent was dry, purified MeCN and 0.1 M $[^nBu_4N][PF_6]$ was used as supporting electrolyte. An internal reference of Cp_2Fe was added at the end of each experiment.

$[Ru(pytpy)_2][PF_6]_2$ was prepared according to the literature method.[8,14]

$[RuL_2][PF_6]_4$ (L^+ = 2–7) general method

$[Ru(pytpy)_2][PF_6]_2$ and approximately 100 molar excess (except for ligand **3**, see below) of the alkylating reagent were dissolved in MeCN (50 cm^3). The reaction mixture was stirred under reflux

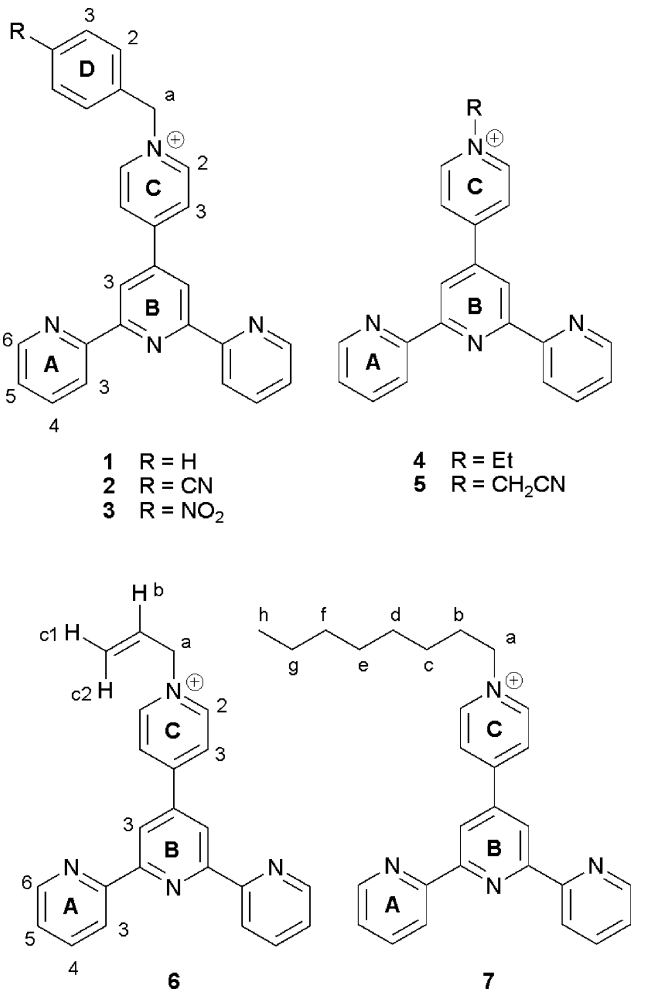

Scheme 1 Ligand structures and labelling for ^{1}H NMR spectroscopic assignments.

for between 3 and 72 h (see below). The reaction was monitored by spot thin layer chromatography until judged to be complete. The volume of solvent was reduced *in vacuo* to ≈5 cm^3 and the product was purified by column chromatography (SiO_2, see below for eluent). The slowest moving, darkest coloured fraction was collected (except in the case of the complex with ligand **7** in which case the fastest moving, darkest coloured fraction was collected) and the MeCN was removed *in vacuo*. Excess aqueous NH_4PF_6 was added to precipitate $[RuL_2][PF_6]_4$ which was collected by filtration over Celite. The product was washed well with H_2O, EtOH and Et_2O, and was removed from the Celite by dissolution in MeCN. Solvent was removed *in vacuo* and $[RuL_2][PF_6]_4$ was isolated as a red powder.

$[Ru(\mathbf{2})_2][PF_6]_4$

$[Ru(pytpy)_2][PF_6]_2$ (180 mg, 0.18 mmol) was treated with 4-(bromomethyl)benzonitrile (4.18 g, 21.4 mmol); reaction time of 12 h; eluent for chromatography MeCN/saturated aqueous KNO_3/H_2O (7 : 2 : 2). Yield: 216 mg, 78.9%. ^{1}H NMR (500 MHz, DMSO-d_6) δ (ppm) 9.77 (s, 4H, H^{B3}), 9.65 (br d, J = 6.3 Hz, 4H, H^{C2}), 9.20 (br d, J = 6.3 Hz, 4H, H^{C3}), 9.10 (d, J = 8.1 Hz, 4H, H^{A3}), 8.17 (t, J = 7.6 Hz, 4H, H^{A4}), 8.05 (d, J = 8.2 Hz, 4H, H^{D3}),

7.82 (d, J = 8.2 Hz, 4H, H^{D2}), 7.59 (d, J = 5.3 Hz, 4H, H^{A6}), 7.34 (m, 4H, H^{A5}), 6.13 (s, 4H, H^{a}). ^{13}C NMR (126 MHz, DMSO-d_6) δ (ppm): 157.4 ($C^{A2/B2}$), 155.4 ($C^{A2/B2}$), 152.5 (C^{A6}), 151.8 (C^{C4}), 146.1 (C^{C2}), 139.9 (C^{B4}), 139.6 (C^{D1}), 138.6 (C^{A4}), 133.2 (C^{D3}), 129.5 (C^{D2}), 128.1 (C^{A5}), 126.0 (C^{C3}), 125.2 (C^{A3}), 122.3 (C^{B3}), 118.4 (C^{D4}), 112.2 ($C^{C\equiv N}$), 62.5 (C^{a}). MALDI-TOF: m/z 1245.0 $[M - 2PF_6]^{2+}$ (calc. 1244.2), 1100.0 $[M - 3PF_6]^{3+}$ (calc. 1099.2). Found: C 41.64, H 2.86, N 8.86; $C_{56}H_{40}F_{24}N_{10}P_4Ru{\cdot}4H_2O$ requires C 41.88, H 3.01, N 8.72%.

$[Ru(3)_2][PF_6]_4$

$[Ru(pytpy)_2][PF_6]_2$ (100 mg, 0.099 mmol) was treated with 4-(bromomethyl)nitrobenzene (0.310 g, 1.43 mmol) (see text); reaction time of 12 h; eluent for chromatography MeCN/saturated aqueous KNO_3/H_2O (7 : 1 : 0.5) made basic with a 5 drops of Et_3N per 100 cm^3 of eluent. Yield: 67.2 mg, 41.6%. ^{1}H NMR (500 MHz, DMSO-d_6) δ (ppm): 9.77 (s, 4H, H^{B3}), 9.66 (d, J = 6.6 Hz, 4H, H^{C2}), 9.21 (d, J = 6.6 Hz, 4H, H^{C3}), 9.09 (d, J = 8.1 Hz, 4H, H^{A3}), 8.41 (d, J = 8.7 Hz, 4H, H^{D3}), 8.17 (t, J = 7.7 Hz, 4H, H^{A4}), 7.90 (d, J = 8.7 Hz, 4H, H^{D2}), 7.59 (d, J = 5.5 Hz, 4H, H^{A6}), 7.34 (m, 4H, H^{A5}), 6.18 (s, 4H, H^{a}). ^{13}C NMR (126 MHz, DMSO-d_6) δ (ppm): 157.6 ($C^{A2/B2}$), 155.6 ($C^{A2/B2}$), 152.0 (C^{C4}), 152.3 (C^{A6}), 145.1 (C^{C2}), 140.1 (C^{B4}), 138.5 (C^{A4}), 141.6 (C^{D1}), 141.3 (C^{D4}), 129.8 (C^{D2}), 128.0 (C^{A5}), 125.8 (C^{C3}), 125.0 (C^{A3}), 124.2 (C^{D3}), 122.1 (C^{B3}), 62.0 (C^{a}). MALDI-TOF: m/z 1431.7 $[M - PF_6]^+$ (calc. 1429.1), 1285.6 $[M - 2PF_6]^+$ (calc. 1284.2), 1150.4 $[Ru(\mathbf{3})(Hpytpy)(PF_6)_2]^+$ (calc. 1149.1), 1005.3 $[Ru(\mathbf{3})(Hpytpy)(PF_6)]^+$ (calc. 1004.2), 995.5 $[M - 4PF_6]^+$ (calc. 994.2), 723.2 $[Ru(pytpy)(Hpytpy)]^+$ (calc. 723.2). Found: C 39.62, H 3.06, N 8.65; $C_{54}H_{40}F_{24}N_{10}P_4Ru{\cdot}3H_2O$ requires C 39.84, H 2.85, N 8.60%.

$[Ru(4)_2][PF_6]_4$

$[Ru(pytpy)_2][PF_6]_2$ (80 mg, 0.079 mmol) was treated with bromoethane (0.90 cm^3, 12 mmol); reaction time of 72 h; eluent for chromatography MeCN/saturated aqueous KNO_3/H_2O (7 : 2 : 2). Yield: 80.6 mg, 64.3%. ^{1}H NMR (500 MHz, DMSO-d_6) δ (ppm): 9.78 (s, 4H, H^{B3}), 9.52 (d, J = 6.6 Hz, 4H, H^{C2}), 9.17 (d, J = 6.6 Hz, 4H, H^{C3}), 9.12 (d, J = 8.1 Hz, 4H, H^{A3}), 8.17 (t, J = 7.9 Hz, 4H, H^{A4}), 7.58 (d, J = 5.5 Hz, 4H, H^{A6}), 7.33 (m, 4H, H^{A5}), 4.80 (q, J = 7.2 Hz, 4H, H^{Et}), 1.73 (t, J = 7.3 Hz, 6H, H^{Et}). ^{13}C NMR (126 MHz, DMSO-d_6) δ (ppm): 157.6 ($C^{A2/B}$), 155.6 ($C^{A2/B2}$), 152.6 (C^{A6}), 150.8 (C^{C4}), 145.4 (C^{C2}), 140.0 (C^{B4}), 138.5 (C^{A4}), 128.0 (C^{A5}), 125.2 (C^{C3}), 125.1 (C^{A3}), 122.0 (C^{B3}), 56.2 (C^{Et}), 16.0 (C^{Et}). MALDI-TOF: m/z 1216.8 $[M - PF_6]^+$ (calc. 1215.1), 1071.6 $[M - 2PF_6]^+$ (calc. 1070.2), 926.8 $[M - 3PF_6]^+$ (calc. 925.2), 782.1 $[M - 4PF_6]^+$ (calc. 780.2). Found: C 36.96, H 2.75, N 8.07; $C_{44}H_{38}F_{24}N_8P_4Ru{\cdot}3H_2O$ requires C 37.38, H 3.14, N 7.93%.

$[Ru(5)_2][PF_6]_4$

$[Ru(pytpy)_2][PF_6]_2$ (100 mg, 0.099 mmol) was treated with bromoacetonitrile (0.66 cm^3, 9.5 mmol); reaction time of 12 h; eluent for chromatography MeCN/saturated aqueous KNO_3/H_2O (7 : 2 : 2). Yield: 67.3 mg, 61.6%. ^{1}H NMR (500 MHz, DMSO-d_6) δ (ppm): 9.80 (s, 4H, H^{B3}), 9.61 (d, J = 6.5 Hz, 4H, H^{C2}), 9.25 (d, J = 6.5 Hz, 4H, H^{C3}), 9.12 (d, J = 8.1 Hz, 4H, H^{A3}), 8.17 (t, J = 7.7 Hz, 4H, H^{A4}), 7.58 (d, J = 5.4 Hz, 4H, H^{A6}), 7.33 (m, 4H, H^{A5}), 6.08 (s, 4H, H^{a}). ^{13}C NMR (126 MHz, DMSO-d_6) δ (ppm): 157.4 ($C^{A2/B2}$), 155.5 ($C^{A2/B2}$), 152.5 (C^{A6+C4}), 146.4 (C^{C2}), 139.5 (C^{B4}), 138.6 (C^{A4}), 128.1 (C^{A5}), 125.4 (C^{C3}), 125.2 (C^{A3}), 122.2 (C^{B3}), 114.3 ($C^{C\equiv N}$), 47.6 (C^{a}). MALDI-TOF: m/z 1092.4 $[M - 2PF_6]^+$ (calc. 1092.1), 1054.6 $[Ru(\mathbf{5})(Hpytpy)(PF_6)_2]^+$ (calc. 1053.1), 947.4 $[M - 3PF_6]^+$ (calc. 947.2), 908.6 $[Ru(\mathbf{5})(Hpytpy)PF_6]^+$ (calc. 908.1), 869.3 $[Ru(Hpytpy)_2PF_6]^+$ (calc. 869.1). Found: C 36.35, H 2.55, N 9.84; $C_{44}H_{32}F_{24}N_{10}P_4Ru{\cdot}4H_2O$ requires C 36.35, H 2.77, N 9.63%.

$[Ru(6)_2][PF_6]_4$

$[Ru(pytpy)_2][PF_6]_2$ (100 mg, 0.099 mmol) was treated with 3-bromoprop-1-ene (1.10 cm^3, 12.7 mmol); reaction time of 4 h; eluent for chromatography MeCN/saturated aqueous KNO_3/H_2O (7 : 2 : 2). Yield: 100.4 mg, 73.2%. ^{1}H NMR (500 MHz, DMSO-d_6) δ (ppm): 9.79 (s, 4H, H^{B3}), 9.48 (d, J = 6.8 Hz, 4H, H^{C2}), 9.19 (d, J = 6.8 Hz, 4H, H^{C3}), 9.12 (d, J = 8.2 Hz, 4H, H^{A3}), 8.17 (t, J = 8.3 Hz, 4H, H^{A4}), 7.58 (d, J = 5.5 Hz, 4H, H^{A6}), 7.33 (m, 4H, H^{A5}), 6.35 (m, 2H, H^{b}), 5.59 (d, J = 10.2 Hz, 2H, H^{c1}), 5.51 (d, J = 17.2 Hz, 2H, H^{c2}), 5.43 (d, J = 5.9 Hz, 4H, H^{a}). ^{13}C NMR (126 MHz, DMSO-d_6) δ (ppm): 157.4 ($C^{A/B2}$), 155.6 ($C^{A2/B2}$), 152.5 (C^{A6}), 151.3 (C^{C4}), 145.7 (C^{C2}), 139.9 (C^{B4}), 138.5 (C^{A4}), 131.5 (C^{b}), 128.0 (C^{A5}), 125.3 (C^{C3}), 125.1 (C^{A3}), 122.1 (C^{B3}), 121.6 (C^{c}), 62.1 (C^{a}). MALDI-TOF: m/z 1240.7 $[M - PF_6]^+$ (calc. 1239.1), 1093.7 $[M - 2PF_6]^+$ (calc. 1094.2), 1055.7 $[Ru(\mathbf{6})(Hpytpy)(PF_6)_2]^+$ (calc. 1054.1), 949.7 $[M - 3PF_6]^+$ (calc. 949.2), 910.6 $[Ru(\mathbf{6})(Hpytpy)(PF_6)]^+$ (calc. 909.2), 764.5 $[Ru(\mathbf{6})(Hpytpy)]^+$ (calc. 764.2). Found: C 38.68, H 2.92, N 8.44; $C_{46}H_{38}F_{24}N_8P_4Ru{\cdot}2H_2O$ requires C 38.91, H 2.98, N 7.89.

$[Ru(7)_2][PF_6]_4$

$[Ru(pytpy)_2][PF_6]_2$ (200 mg, 0.198 mmol) was treated with 1-bromooctane (3.0 cm^3, 17 mmol); reaction time of 48 h; eluent for chromatography MeCN/saturated aqueous KNO_3/H_2O (10 : 0.5 : 1.5). Yield: 121.7 mg, 38.4%. ^{1}H NMR (500 MHz, CD_3CN) δ (ppm): 9.14 (s, 4H, H^{B3}), 9.01 (d, J = 6.6 Hz, 4H, H^{C2}), 8.77 (d, J = 6.5 Hz, 4H, H^{C3}), 8.70 (d, J = 8.1 Hz, 4H, H^{A3}), 8.02 (t, J = 7.9 Hz, 4H, H^{A4}), 7.46 (d, J = 5.5 Hz, 4H, H^{A6}), 7.25 (m, 4H, H^{A5}), 4.69 (t, J = 7.6 Hz, 4H, H^{a}), 2.13 (m, 4H, H^{b}), 1.46 (m, 8H, H^{c+d}), 1.35 (m, 12H, H^{e+f+g}), 0.93 (t, J = 6.7 Hz, 6H, H^{h}). ^{13}C NMR (126 MHz, CD_3CN) δ (ppm): 158.4 ($C^{A2/B2}$), 157.0 ($C^{A2/B2}$), 153.8 (C^{A6}), 153.7 (C^{C4}), 146.4 (C^{C2}), 142.2 (C^{B4}), 139.5 (C^{A4}), 129.0 (C^{A5}), 127.5 (C^{C3}), 126.0 (C^{A3}), 123.3 (C^{B3}), 62.7 (C^{a}), 32.3 ($C^{e/f/g}$), 31.7 (C^{b}), 29.5 ($C^{e/f/g}$), 29.4 ($C^{e/d}$), 26.5 ($C^{e/d}$), 23.0 ($C^{e/f/g}$), 14.1 (C^{h}). MALDI-TOF: m/z 1384.1 $[M - PF_6]^+$ (calc. 1383.3), 1239.6 $[M - 2PF_6]^+$ (calc. 1238.3), 1094.5 $[M - 3PF_6]^+$ (calc. 1093.4). Found: C 42.28, H 4.26, N 7.24; $C_{56}H_{62}F_{24}N_8P_4Ru{\cdot}3H_2O$ requires C 42.51, H 4.33, N 7.08.

$[RuL_2][HSO_4]_4$ (L^+ = 1–7) general method

One equivalent (see below for scale) of $[RuL_2][PF_6]_4$ (L^+ = **1–7**) was stirred with four equivalents of $[^tBu_4N][HSO_4]$ in a mixture of MeCN and CH_2Cl_2 (9 : 1 by volume) for 30 min during which time a precipitate formed. The precipitate was filtered over Celite, washed with MeCN and then removed from the Celite by dissolution in deionised water. The water was removed under reduced pressure to yield a red powder, and the product was then stirred in boiling MeCN for 20 min to remove any remaining $[^tBu_4N][PF_6]$. After filtration through a glass sinter, the solid

residue was washed with EtOH and Et_2O, and each product was isolated as a red powder.

[Ru(1)$_2$][HSO$_4$]$_4$

[Ru(**1**)$_2$][PF$_6$]$_4$ (174 mg, 0.117 mmol) gave [Ru(**1**)$_2$][HSO$_4$]$_4$ (150 mg, 0.116 mmol, 99.1%). ^{1}H NMR (500 MHz, D_2O) δ (ppm): 9.25 (s, 4H, H^{B3}), 9.21 (d, J = 5.3 Hz, 4H, H^{C2}), 8.81 (d, J = 5.3 Hz, 4H, H^{C3}), 8.68 (d, J = 7.7 Hz, H^{A3}), 7.95 (t, J = 7.3 Hz, 4H, H^{A4}), 7.59 (m, 4H, H^{D2}), 7.56 (m, 6H, H^{D3+D4}), 7.42 (d, J = 5.2 Hz, 4H, H^{A6}), 7.18 (m, 4H, H^{A5}), 5.97 (s, 4H, H^a). ^{13}C NMR (126 MHz, D_2O) δ (ppm): 160.0 (C$^{A2/B2}$), 158.8 (C$^{A2/B2}$), 156.0 (C^{C4}), 154.9 (C^{A6}), 148.0 (C^{C2}), 143.7 (C^{B4}), 141.2 (C^{A4}), 135.4 (C^{D1}), 132.9 (C^{D4}), 132.5 (C^{D3}), 132.1 (C^{D2}), 130.5 (C^{A5}), 129.2 (C^{C3}), 127.6 (C^{A3}), 124.6 (C^{B3}), 67.3 (C^a). MALDI-TOF: m/z 1193.1 [M – HSO$_4$]$^+$ (calc. 1195.1). Elemental analysis (see text).

[Ru(2)$_2$][HSO$_4$]$_4$

[Ru(**2**)$_2$][PF$_6$]$_4$ (80.0 mg, 0.0522 mmol) gave [Ru(**2**)$_2$][HSO$_4$]$_4$ (41.7 mg, 0.0311 mmol, 59.6%). ^{1}H NMR (500 MHz, D_2O) δ (ppm): 9.28 (s, 4H, H^{B3}), 9.25 (d, J = 5.6 Hz, 4H, H^{C2}), 8.87 (d, J = 5.6 Hz, 4H, H^{C3}), 8.70 (d, J = 7.9 Hz, H^{A3}), 7.97 (t, J = 7.6 Hz, 4H, H^{A4}), 7.94 (d, J = 8.1 Hz, 4H, H^{D3}), 7.73 (d, J = 8.0 Hz, 4H, H^{D2}), 7.44 (d, J = 5.2 Hz, 4H, H^{A6}), 7.20 (m, 4H, H^{A5}), 6.09 (s, 4H, H^a). ^{13}C NMR (126 MHz, D_2O) δ (ppm): 160.1 (C$^{A2/B2}$), 158.8 (C$^{A2/B2}$), 155.0 (C^{A6}), 148.4 (C^{C2}), 131.2 (C^{A4}), 140.7 (C^{D1}), 136.4 (C^{D3}), 132.4 (C^{D2}), 130.6 (C^{A5}), 129.4 (C^{C3}), 127.7 (C^{A3}), 124.7 (C^{B3}), 122.7 (C$^{C\equiv N}$), 115.4 (C^{D4}), 66.5 (C^a), (C^{B4} and C^{C4} not resolved). MALDI-TOF: m/z 839.0 [Ru(**2**)(Hpytpy)]$^+$ (calc. 839.2), 723.9 [Ru(pytpy)(Hpytpy)]$^+$ (calc. 723.2). Found: C 46.42, H 3.60, N 10.00; $C_{56}H_{44}N_{10}O_{16}RuS_4\cdot 6H_2O$ requires C 46.37, H 3.89, N 9.66 (see text).

[Ru(3)$_2$][HSO$_4$]$_4$

[Ru(**3**)$_2$][PF$_6$]$_4$ (267 mg, 0.170 mmol) gave [Ru(**3**)$_2$][HSO$_4$]$_4$ (230 mg, 0.166 mmol, 97.9%). ^{1}H NMR (500 MHz, D_2O) δ (ppm): 9.29 (s, 4H, H^{B3}), 9.27 (d, J = 6.4 Hz, 4H, H^{C2}), 8.88 (d, J = 5.5 Hz, 4H, H^{C3}), 8.70 (d, J = 7.8 Hz, H^{A3}), 8.39 (d, J = 8.2 Hz, 4H, H^{D3}), 7.97 (t, J = 7.6 Hz, 4H, H^{A4}), 7.80 (d, J = 8.2 Hz, 4H, H^{D2}), 7.44 (d, J = 4.7 Hz, 4H, H^{A6}), 7.20 (m, 4H, H^{A5}), 6.14 (s, 4H, H^a). ^{13}C NMR (126 MHz, D_2O) δ (ppm): 160.0 (C$^{A2/B2}$), 158.8 (C$^{A2/B2}$), 154.9 (C^{A6}), 151.4 (C^{D4}), 148.5 (C^{C2}), 143.5 (C^{D1}), 141.2 (C^{A4}), 132.9 (C^{D2}), 130.5 (C^{A5}), 129.5 (C^{C3}), 127.7 (C^{A3}), 127.4 (C^{D3}), 124.7 (C^{B3}), 66.1 (C^a), (C^{B4} and C^{C4} not resolved). MALDI-TOF: 1001.6 [M – 3HSO$_4$]$^+$ (calc. 1001.1), 724.0 [Ru(Hpytpy)$_2$]$^+$ (calc. 724.2) Found: C 42.42, H 3.64, N 9.32; $C_{54}H_{44}N_{10}O_{20}RuS_4\cdot 8H_2O$ requires C 42.49, H 3.96, N 9.18 (see text).

[Ru(4)$_2$][HSO$_4$]$_4$

[Ru(**4**)$_2$][PF$_6$]$_4$ (304 mg, 0.223 mmol) gave [Ru(**4**)$_2$][HSO$_4$]$_4$ (257 mg, 0.220 mmol, 98.7%). ^{1}H NMR (500 MHz, D_2O) δ (ppm): 9.27 (s, 4H, H^{B3}), 9.18 (d, J = 6.3 Hz, 4H, H^{C2}), 8.81 (d, J = 6.4 Hz, 4H, H^{C3}), 8.69 (d, J = 7.9 Hz, H^{A3}), 7.96 (t, J = 7.8 Hz, 4H, H^{A4}), 7.44 (d, J = 5.1 Hz, 4H, H^{A6}), 7.20 (m, 4H, H^{A5}), 4.80 (coincident with solvent, H^{Et}), 1.75 (t, J = 7.3 Hz, 6H, H^{Et}). ^{13}C NMR (126 MHz, D_2O) δ (ppm): 160.0 (C$^{A2/B2}$), 158.8 (C$^{A2/B2}$), 155.5 (C^{C4}), 154.9 (C^{A6}), 147.7 (C^{C2}), 143.9 (C^{B4}), 141.1 (C^{A4}), 130.5 (C^{A5}), 129.1 (C^{C3}), 127.6 (C^{A3}), 124.6 (C^{B3}), 60.0 (C^{Et}), 18.4 (C^{Et}). MALDI-TOF: m/z 850.4 [Ru(**4**)(Hpytpy)(HSO$_4$)]$^+$ (calc. 849.2), 821.4 [Ru(Hpytpy)$_2$(HSO$_4$)]$^+$ (calc. 821.1), 751.3 [Ru(**4**)(Hpytpy)(HSO$_4$)]$^+$ (calc. 752.2), 723.3 [Ru(pytpy)-(Hpytpy)]$^+$ (calc. 723.2). Elemental analysis (see text).

[Ru(5)$_2$][HSO$_4$]$_4$

[Ru(**5**)$_2$][PF$_6$]$_4$ (163 mg, 0.118 mmol) gave [Ru(**5**)$_2$][HSO$_4$]$_4$ (92.5 mg, 0.0778 mmol, 65.9%). ^{1}H NMR (500 MHz, D_2O) δ (ppm): 9.36 (d, J = 6.5 Hz, 4H, H^{C2}), 9.33 (s, 4H, H^{B3}), 8.98 (d, J = 6.6 Hz, 4H, H^{C3}), 8.72 (d, J = 8.1 Hz, H^{A3}), 7.98 (t, J = 7.5 Hz, 4H, H^{A4}), 7.45 (d, J = 5.3 Hz, 4H, H^{A6}), 7.21 (m, 4H, H^{A5}), 6.09 (s, 4H, H^a). ^{13}C NMR (126 MHz, D_2O) δ (ppm): 159.9 (C$^{A2/B2}$), 158.8 (C$^{A2/B2}$), 157.7 (C^{C4}), 154.9 (C^{A6}), 148.6 (C^{C2}), 143.1 (C^{B4}), 141.2 (C^{A4}), 130.5 (C^{A5}), 129.6 (C^{C3}), 127.7 (C^{A3}), 124.7 (C^{B3}), 116.6 (C$^{C\equiv N}$), 50.5 (C^a). MALDI-TOF: m/z 859.8 [Ru(**5**)(pytpy)(HSO$_4$)]$^+$ (calc. 859.1),761.6 [Ru(**5**)(pytpy)]$^+$ (calc. 762.2), 722.3 [Ru(pytpy)$_2$]$^+$ (calc. 722.2). Elemental analysis (see text).

[Ru(6)$_2$][HSO$_4$]$_4$

[Ru(**6**)$_2$][PF$_6$]$_4$ (210 mg, 0.152 mmol) gave [Ru(**6**)$_2$][HSO$_4$]$_4$ (148 mg, 0.124 mmol, 81.6%). ^{1}H NMR (500 MHz, D_2O) δ (ppm): 9.28 (s, 4H, H^{B3}), 9.16 (d, J = 5.9 Hz, 4H, H^{C2}), 8.84 (d, J = 5.8 Hz, 4H, H^{C3}), 8.70 (d, J = 7.9 Hz, 4H, H^{A3}), 7.97 (t, J = 7.6 Hz, 4H, H^{A4}), 7.45 (d, J = 5.3 Hz, 4H, H^{A6}), 7.21 (m, 4H, H^{A5}), 6.27 (m, 2H, H^b), 5.66 (d, J = 10.3 Hz, 2H, H^{c1}), 5.63 (d, J = 17.2 Hz, 2H, H^{c2}), 5.39 (d, J = 6.1 Hz, 4H, H^a). ^{13}C NMR (126 MHz, D_2O) δ (ppm): 160.0 (C$^{A2/B2}$), 158.8 (C$^{A2/B2}$), 156.0 (C^{C4}), 154.9 (C^{A6}), 148.0 (C^{C2}), 143.8 (C^{B4}), 141.2 (C^{A4}), 132.6 (C^b), 130.5 (C^{A5}), 129.1 (C^{C3}), 127.7 (C^{A3}), 126.2 (C^c), 124.6 (C^{B3}), 66.1 (C^a). MALDI-TOF: m/z 803.2 [Ru(**6**)$_2$]$^+$ (calc. 804.2), 763.2 [Ru(**6**)(pytpy)]$^+$ (calc. 763.2), 724.0 [Ru(Hpytpy)$_2$]$^+$ (calc. 724.2). Found: C 42.84, H 3.65, N 8.99; $C_{46}H_{42}N_8O_{16}RuS_4\cdot 5H_2O$ requires C 43.09, H 4.09, N 8.74 (see text).

[Ru(7)$_2$][HSO$_4$]$_4$

[Ru(**7**)$_2$][PF$_6$]$_4$ (58 mg, 0.038 mmol) gave [Ru(**7**)$_2$][HSO$_4$]$_4$ (35 mg, 0.026 mmol, 68%). ^{1}H NMR (500 MHz, CD_3CN) δ (ppm): 9.29 (s, 4H, H^{B3}), 9.17 (d, J = 6.4 Hz, 4H, H^{C2}), 8.83 (d, J = 6.4 Hz, 4H, H^{C3}), 8.71 (d, J = 8.1 Hz, 4H, H^{A3}), 7.98 (t, J = 7.8 Hz, 4H, H^{A4}), 7.45 (d, J = 5.4 Hz, 4H, H^{A6}), 7.21 (m, 4H, H^{A5}), 4.78 (t, overlapping solvent, H^a), 2.13 (m, 4H, H^b), 1.44 (m, 8H, H^{c+d}), 1.34–1.30 (overlapping m, 12H, H^{e+f+g}), 0.87 (t, J = 6.8 Hz, 6H, H^h). ^{13}C NMR (126 MHz, CD_3CN) δ (ppm): 160.0 (C$^{A2/B2}$), 158.8 (C), 155.5 (C^{C4}), 154.8 (C^{A6}), 147.9 (C^{C2}), 143.8 (C^{B4}), 141.1 (C^{A4}), 130.4 (C^{A5}), 129.0 (C^{C3}), 127.6 (C^{A3}), 124.6 (C^{B3}), 64.7 (C^a), 33.7 (C$^{e/f/g}$), 33.4 (C^b), 30.9 (C$^{c/d}$), 30.8 (C$^{e/f/g}$), 28.1 (C$^{c/d}$), 24.7 (C$^{e/f/g}$), 16.2 (C^h). MALDI-TOF: m/z 1237.8 [M – HSO$_4$]$^+$ (calc. 1239.3), 949.6 [M – 4HSO$_4$]$^{4+}$ (calc. 948.4), 723.3 [Ru(pytpy)(Hpytpy)]$^{3+}$ (calc. 723.2). Elemental analysis (see text).

Crystal structure determinations

Data were collected on a Stoe IPDS diffractometer; data reduction, solution and refinement used Stoe IPDS software[16] and SHELXL97.[17] ORTEP figures were drawn using Ortep-3 for

Windows,[18] and structures have been analysed using Mercury v. 2.3.[19,20]

$[Ru(4)_2][PF_6]_4 \cdot H_2O$

$C_{44}H_{40}F_{24}N_8OP_4Ru$, M = 1377.79, red needle, monoclinic, space group $P2_1/c$, a = 18.322(4), b = 8.8509(18), c = 31.688(6) Å, β = 95.16(3)°, U = 5117.9(18) Å^3, Z = 4, D_c = 1.786 mg m^{-3}, μ(Mo-Kα) = 0.565 mm^{-1}, T = 173 K. Total 84418 reflections, 11159 unique, R_{int} = 0.1627. Refinement of 8456 reflections (925 parameters) with $I > 2\sigma(I)$ converged at final R_1 = 0.0664 ($R1$ all data = 0.0935), wR_2 = 0.1280 ($wR2$ all data = 0.1385), GOF = 1.161.

Computational methods

Complexes $[RuL_2]^{4+}$ with L^+ = **1–7** and $[Ru(pytpy)_2]^{2+}$ were modelled using TD-DFT implemented in the Gaussian 09 program.[21] Each complex was initially geometry-optimized using the RHF method with a 3-21G basis set applied to non-metal atoms, and the Los Alamos National Laboratory 2 double ζ (LANL2DZ) effective core potential[22] (ECP) used to describe the Ru^{2+} centre. A double-zeta Ru basis set[22] associated with the LANL2DZ ECP was taken from the Basis Set Exchange.[23] The ECP and basis set were defined explicitly in Gaussian 09 (see ESI†) using the 'GEN' and 'Pseudo = Read' keywords. Frequency calculations were performed at this level of theory for each complex to confirm the identification of a local minimum energy structure. Further refinement of complex geometries followed using the B3LYP hybrid density functional[24] and a larger 6-31G(d) basis set for non-metal atoms, with the same Ru^{2+} ECP/basis set combination as before. The Integral Equation Formalism polarizable continuum model[25–28] (PCM) was used during geometry optimization and for subsequent TD-DFT calculations to describe solvation of each complex in MeCN to more closely match the experimental conditions. A similar level of calculation has been applied to a series of $[Ru(tpy_2)]^{2+}$ complexes,[29] and the general reliability of the LANL2DZ ECP combined with the B3LYP hybrid density functional for transition metal complexes has been highlighted.[30] Predicted TD-DFT UV-VIS transitions were calculated at the B3LYP level, and simulated spectra were generated from Gaussian 09 output using the GaussSum program.[31] Grids containing orbital densities were written as 'cube' files by Gaussian 09, and were used to generate isodensity surfaces for selected MOs using the VMD program.[32]

Results and discussion

Synthesis and characterization of $[RuL_2][PF_6]_4$

The *N*-substituents were chosen to give a range of electron-donating and electron-withdrawing groups, our intention being to investigate the effects of the substituents on the electrochemical and photophysical properties of the $\{Ru(tpy)_2\}$ core. The complexes $[RuL_2][PF_6]_4$ with L^+ = **2–7** (Scheme 1) were synthesized by treating $[Ru(pytpy)_2][PF_6]_2$[8,14] with an excess of the appropriate alkylating agent in MeCN under reflux. Typically, around a 100-fold excess of alkylating agent was used to ensure complete alkylation of both pendant pyridine rings. However, in the case of ligand **3**, problems were encountered chromatographically separating the excess ligand from the ruthenium(II) complex and the best results were obtained using only a 10-fold excess of ligand. Reactions were monitored by spot TLC. The burgundy red colour of the bisalkylated complex was readily distinguished from the orange-red colours of the starting complex and monoalkylated complex, respectively. After workup, each $[RuL_2][PF_6]_4$ complex was isolated as a red powder in moderate to good yield. Unreacted starting material accounted for the remaining ruthenium-containing material, except in the case of ligand **7** where a significant amount of monoalkylated product was observed. No attempt was made to purify this by-product. Diagnostic peaks in the MALDI mass spectra of the product arose from the $[M - PF_6]^+$, $[M - 2PF_6]^+$ and $[M - 3PF_6]^+$ ions. Fragmentation by loss of the alkyl substituents was observed in some cases, giving rise to the ions $[RuL(Hpytpy)(PF_6)_2]^+$, $[RuL(Hpytpy)PF_6]^+$, $[RuL(Hpytpy)]^+$, $[Ru(Hpytpy)_2PF_6]^+$ and $[Ru(Hpytpy)_2]^+$

The appearance of only one set of tpy signals in the ^{1}H and ^{13}C NMR spectra of each complex was in accord with the alkylation of both pendant pyridine nitrogen atoms. The spectra were assigned by COSY, NOESY, HMQC and HMBC techniques. Protons H^{C2} and H^{C3} were distinguished by the observation of NOESY crosspeaks between the signals for H^{B3} and H^{C3}, and for H^a and H^{C2}. For compounds $[Ru(\mathbf{2})_2][PF_6]_4$ and $[Ru(\mathbf{3})_2][PF_6]_4$, protons H^{D2} and H^{D3} were unambiguously assigned from the H^a–H^{D2} NOESY cross peaks. Differences in the solubilities of the complexes prevented the spectra from being recorded in a common solvent. However, $[Ru(\mathbf{7})_2][PF_6]_4$ and $[Ru(pytpy)_2][PF_6]_2$[8,14] were both soluble in CD_3CN, and their spectra can be directly compared. Upon alkylation, the resonances for the protons in the outer tpy rings A are little affected, while that for H^{B3} shifts to higher frequency (δ 9.07 to 9.14 ppm on going from $[Ru(pytpy)_2][PF_6]_2$ to $[Ru(\mathbf{7})_2][PF_6]_4$). The most significant perturbation is seen for H^{C2} (adjacent to the position of alkylation) which shifts from δ 8.14 to 9.01 ppm. The signal for proton H^{C3} shifts to lower frequency (δ 8.97 to 8.77 ppm). A similar pattern of signals for ring A, B and C protons is observed for each of the alkylated derivatives. A comparison of the ^{1}H NMR spectra for DMSO-d_6 solutions of $[RuL_2][PF_6]_4$ with L^+ = **2–6**, revealed negligible perturbation of the chemical shifts for the tpy protons. The closer proximity of protons H^{C2} and H^{C3} to the *N*-substituent resulted in small, but significant, changes in their chemical shift values.

X-ray quality crystals of $[Ru(\mathbf{4})_2][PF_6]_4 \cdot H_2O$ were grown by diffusion of Et_2O vapour into an acetone solution of the complex. The structure determination confirmed ethylation at both pendant pyridine sites. The structure of the $[Ru(\mathbf{4})_2]^{4+}$ cation is depicted in Fig. 1, and selected bond distances and angles are listed in the caption. The coordination sphere of the ruthenium(II) ion is unexceptional. The N4–C21 and N8–C43 bond lengths of 1.487(19) and 1.486(6) Å, respectively, are consistent with single bonds between each pendant pyridine N atom and the ethyl group. One ethyl group is disordered and has been modelled over sites with fractional occupancies 0.76 and 0.24; only the major occupancy sites are shown in Fig. 1. The two pendant pyridine rings are twisted with respect to one another, the angle between the least squares planes through the rings being 76.4(3)°. The N4···Ru1···N8 deviates slightly from linearity, and the corresponding angle of 171.47(5)° compares favourably with those in related compounds, with the exception of those which are constrained to 180° by crystallographic symmetry.[33–36]

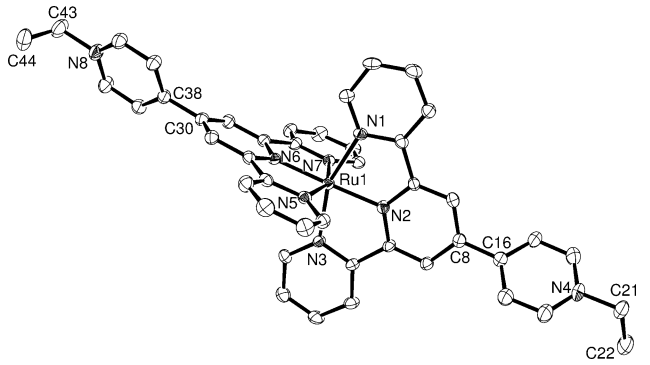

Fig. 1 Structure of the $[Ru(\mathbf{4})_2]^{4+}$ cation in $[Ru(\mathbf{4})_2][PF_6]_4 \cdot H_2O$ with ellipsoids plotted at the 40% probability level; H atoms are omitted for clarity. The ethyl group containing C21/C22 is disordered (see text) and only major occupancy sites are shown. Selected bond parameters: Ru1–N1 = 2.076(3), Ru1–N2 = 1.981(3), Ru1–N3 = 2.088(3), Ru1–N5 2.082(4), Ru1–N6 = 1.976(3), Ru1–N7 = 2.075(4), N4–C21 = 1.487(19), N8–C43 1.486(6) Å; N2–Ru1–N1 = 79.37(14), N2–Ru1–N3 = 78.44(14), N5–Ru1–N6 = 78.70(14), N6–Ru1–N7 = 78.95(14)°.

The $[Ru(\mathbf{4})_2]^{4+}$ cations pack with a combination of face-to-face and edge-to-face embraces (Fig. 2a). This leaves the *N*-ethylpyridine units directed above and below the $\{Ru(tpy)_2\}$-domains, and the former intermesh with one another as shown in Fig. 2b. These packing motifs are a familiar feature of $[Ru(tpy)_2]^{2+}$ complexes bearing 4′-pyridyl or 4′-aryl substituents.[37–40] Three of the four hexafluoridophosphate counter-ions are disordered and have been modelled with site occupancies of 0.68/0.32, 0.80/0.20 and 0.55/0.45, respectively. There are extensive CH···F packing interactions throughout the lattice. The water molecule is disordered over two positions (0.60 : 0.40), and the H atoms were not located. No meaningful comments about the role of the water in packing can therefore be made.

Single crystals of $[Ru(\mathbf{3})_2][PF_6]_4 \cdot x MeNO_2$ were grown from a nitromethane solution of the complex layered with Et_2O. X-ray diffraction data confirmed the $[Ru(\mathbf{3})_2][PF_6]_4$ formulation. In the $[Ru(\mathbf{3})_2]^{4+}$ cation, the Ru atom is octahedrally sited, being bound through the tpy domains of two $[\mathbf{3}]^+$ ligands. The cation suffers from severe positional disorder of the two pendant 4-nitrobenzyl substituents. It was possible to resolve the disorder by going to a unit cell containing eight cations (four independent cations in space group $P\bar{1}$), but the structure was so large that the 1412 independent atoms could not be refined to a satisfactory level using traditional small-molecule crystallographic software.

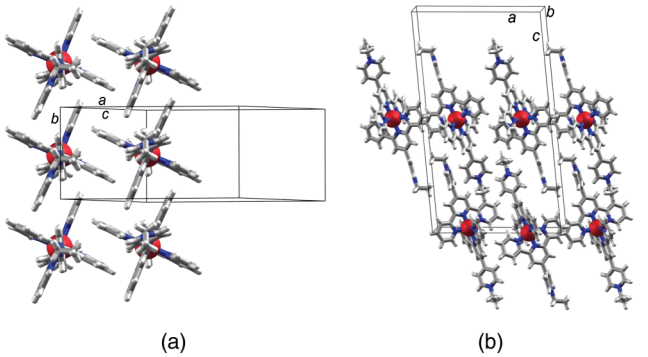

Fig. 2 (a) Face-to-face and edge-to-face interactions between tpy domains in the cations in $[Ru(\mathbf{4})_2][PF_6]_4 \cdot H_2O$, and (b) intermeshing of the *N*-ethylpyridine units.

Electronic absorption and emission spectra of $[RuL_2][PF_6]_4$

Fig. 3 shows the electronic absorption spectra of the complexes. We have previously noted that conversion of $[Ru(pytpy)_2][PF_6]_2$ to $[Ru(N\text{-}Mepytpy)_2][PF_6]_4$ or to $[Ru(\mathbf{1})_2][PF_6]_4$ (see Scheme 1) results in a red shift of the MLCT band from 488 to 507 or 511 nm (MeCN solution).[8,14] A comparable red shift is observed on going from $[Ru(pytpy)_2][PF_6]_2$ to the *N*-alkylated complexes studied here (Table 1). Fig. 3 illustrates that, irrespective of the *N*-substituent, the spectra both in the visible and UV regions are similar. The fact that there is essentially no variation in the energy of the MLCT band suggests that the character of the ligand orbital involved in

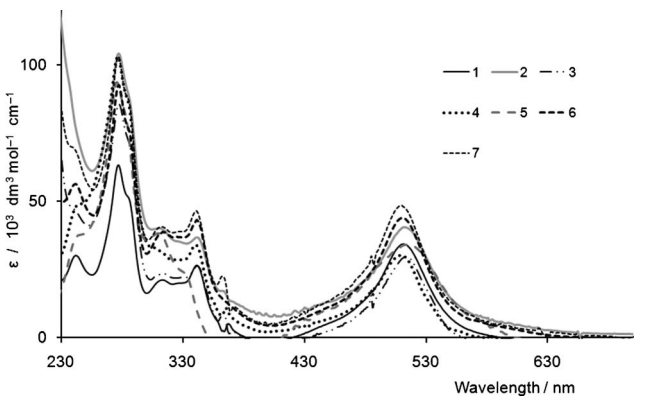

Fig. 3 Electronic absorption spectra of MeCN solutions of $[RuL_2][PF_6]_4$ where L^+ = ligands **1** to **7**. The absorption data are given in Table 1.

Table 1 UV-Vis spectroscopic data. All data refer to hexafluoridophosphate salts in MeCN solution

Complex	MLCT/nm (ε/10³ dm³ mol⁻¹ cm⁻¹)	Ligand-centred π*←π/nm (ε/10³ dm³ mol⁻¹ cm⁻¹)				
$[Ru(pytpy)_2]^{2+}$[a]	488 (30.9)	312 (61.6)			273 (78.4)	238 (43.5)
$[Ru(\mathbf{1})_2]^{4+}$[b]	511 (34.3)	341 (26.4)	313 (21.1)	292 sh (46.8)	277 (63.3)	241 (29.9)
$[Ru(\mathbf{2})_2]^{4+}$	512 (40.6)	341 (36.8)	312 (40.6)	285 sh (87.6)	277 (104.2)	
$[Ru(\mathbf{3})_2]^{4+}$	513 (29.7)	342 (26.3)	312 (23.3)	288 sh (68.0)	277 (85.7)	240 sh (46.2)
$[Ru(\mathbf{4})_2]^{4+}$	509 (30.3)	341 (34.0)	309 sh (29.6)	284 sh (88.4)	276 (103.0)	241 sh (47.3)
$[Ru(\mathbf{5})_2]^{4+}$	513 (34.2)	330 sh (24.2)	309 (39.9)	284 sh (77.7)	275 (93.7)	242 sh (36.9)
$[Ru(\mathbf{6})_2]^{4+}$	510 (44.0)	341 (43.3)	313 (38.9)	285 sh (76.6)	277 (92.7)	241 (56.4)
$[Ru(\mathbf{7})_2]^{4+}$	510 (48.7)	341 (46.7)	313 (40.6)	285 sh (87.6)	277 (103.4)	240 sh (69.6)

[a] Ref. 8; [b] Ref. 14

Table 2 Emission maxima, λ_{em} (λ_{ex} = 510 nm), lifetimes, τ, (475 nm laser diode) and quantum yields, Φ, for hexafluoridophosphate salts in MeCN solution at room temperature

Complex	λem/nm	τ/ns	Φ (±15%)
$[Ru(\mathbf{1})_2]^{4+}$	728	160	0.0073
$[Ru(\mathbf{2})_2]^{4+}$	741	115	0.0038
$[Ru(\mathbf{3})_2]^{4+}$	730	105	0.0001
$[Ru(\mathbf{4})_2]^{4+}$	715	162	0.0035
$[Ru(\mathbf{5})_2]^{4+}$	703	129	0.0005
$[Ru(\mathbf{6})_2]^{4+}$	727	145	0.0045
$[Ru(\mathbf{7})_2]^{4+}$	701	166	0.0044

Table 3 Redox potentials for $[RuL_2][PF_6]_4$ (L^+ = **1–7**) compared to $[Ru(pytpy)_2][PF_6]_2$ (all in MeCN solution) and *vs.* Fc^+/Fc. Processes are reversible unless otherwise stated

Complex	Ru^{2+}/Ru^{3+}/V	Ligand-centred reductions/V			
$[Ru(pytpy)_2]^{2+}$[a]	0.95	−1.54	−1.80		
$[Ru(\mathbf{1})_2]^{4+}$	1.01	−1.08	−1.46	−1.75	
$[Ru(\mathbf{2})_2]^{4+}$	1.02	−1.01	−1.50	−1.73	
$[Ru(\mathbf{3})_2]^{4+}$	1.05	−1.10	−1.40	−1.69[b]	−2.22[b]
$[Ru(\mathbf{4})_2]^{4+}$	1.00	−1.09	−1.56	−1.79	
$[Ru(\mathbf{5})_2]^{4+}$	1.02	−0.96	−1.40	−1.60[c]	−1.99[b]
$[Ru(\mathbf{6})_2]^{4+}$	1.02	−1.05	−1.33	−1.76	
$[Ru(\mathbf{7})_2]^{4+}$	1.00	−1.08	−1.56	−1.79[c]	−1.94[b]

[a] Ref. 8; [b] Irreversible; [c] Quasi-reversible.

the transition does not contain character from the *N*-substituent. This is consistent with the *N*–CH_2 group preventing delocalization of π-character from the pendant pyridine ring to the *N*-substituent. We return to this in the TD-DFT study presented later.

All the $[RuL_2][PF_6]_4$ complexes (L^+ = **1–7**) are emissive in MeCN solution. Excitation in the MLCT band (λ_{ex} = 510 nm) resulted in an emission close to 720–730 nm. The data are summarized in Table 2. The complexes exhibit emission lifetimes of between 105 and 166 ns. The longest lived emitters were the *N*-ethyl, *N*-octyl and *N*-benzyl derivatives, while the presence of the cyano or nitro functionalities decreases the lifetime.

Redox behaviour of $[RuL_2][PF_6]_4$

All of the $[RuL_2][PF_6]_4$ complexes (L^+ = **2–7**) are electrochemically active in MeCN solution and were studied by cyclic and square wave voltammetry. Each complex undergoes a fully reversible one-electron Ru^{2+}/Ru^{3+} redox process, in addition to multiple, ligand centred reductions (Table 3). On going from $[Ru(tpy)_2]^{2+}$ to $[Ru(pytpy)_2]^{2+}$, the potential of the Ru^{2+}/Ru^{3+} redox couple shifts from 0.92 to 0.95 V, and a more significant shift (to ≈1.0 V) is observed upon protonation or methylation of the pendant pyridine rings.[8] The Ru^{2+}/Ru^{3+} potentials in Table 3 show no variation within experimental error, despite the introduction of both electron-withdrawing and electron-donating *N*-substituents.

Synthesis and characterization of $[RuL_2][HSO_4]_4$

The $[RuL_2][PF_6]_4$ salts are insoluble in water, which renders them unsuitable for application as photosensitizers in homogenous water oxidation systems. For L^+ = 4′-(4-methylpyridinio)-2,2′:6′,2′-terpyridine, we have overcome this problem by exchanging the $[PF_6]^-$ anion for $[HSO_4]^-$.[15] Treatment of $[RuL_2][PF_6]_4$ (L = **1–7**) with four equivalents of $[^tBu_4N][HSO_4]$ in a mixture of MeCN and CH_2Cl_2 resulted in the formation of dark red solids which were insoluble in common organic solvents (*e.g.* MeCN, CH_2Cl_2, EtOH, Et_2O), but readily soluble in water. MALDI mass spectrometric data were consistent with the formation of hydrogensulfate salts. The spectra also demonstrated loss of the *N*-substituents, with the base peaks appearing at *m*/*z* 722, 723 or 724 in all of the spectra. The latter peaks were assigned to the $[Ru(pytpy)_2]^+$, $[Ru(pytpy)(Hpytpy)]^+$ or $[Ru(Hpytpy)_2]^+$ ions. ^{31}P NMR spectroscopic data of several of the samples confirmed the absence of $[PF_6]^-$ in the bulk material.

Attempts to obtain satisfactory elemental analysis on the hydrogensulfate salts were either unsuccessful or the data indicated the formation of hydrates, *e.g.* $[Ru(\mathbf{2})_2][HSO_4]_4{\cdot}6H_2O$ and $[Ru(\mathbf{3})_2][HSO_4]_4{\cdot}8H_2O$. That the salts are hygroscopic is not surprising given the high probability of $[HSO_4]^-$ forming hydrogen bonds in the solid state. TGA-MS analysis of a sample of $[Ru(\mathbf{3})_2][HSO_4]_4$ showed an initial 2.3% weight loss (≤200 °C) followed by two further steps of water loss (2.4 and 4.7% weight loss between 200 and 400 °C). Sample decomposition occurred at higher temperatures. The initial degradation steps correspond to loss of $2H_2O$, $2H_2O$ and $4H_2O$, consistent with the elemental analytical data.

^1H and ^{13}C NMR spectra of $[RuL_2][HSO_4]_4$ (L^+ = **1–7**) were recorded in D_2O. The ^{13}C NMR spectra were referenced with respect to $Na[Me_3Si(CH_2)_3SO_3]$ (DSS)[41] with the $SiMe_3$ signal at δ 0.0 ppm. The ^1H and ^{13}C NMR spectra were assigned by COSY, HMQC and HMBC methods. In both $[Ru(\mathbf{4})_2][HSO_4]_4$ and $[Ru(\mathbf{7})_2][HSO_4]_4$, the signal for the *N*–CH_2 protons was coincident with the signal for residual HOD, but could be assigned from a crosspeak in the HMQC spectrum. For each complex, the ^1H and ^{13}C NMR spectra were consistent with one ligand environment and the presence of the desired homoleptic complex. The combined effects of changing the anion and the solvent (from CD_3CN to D_2O) can be assessed by considering values of $\Delta\delta$, defined as $\delta([PF_6]^-$ salt) − $\delta([HSO_4]^-$ salt), for each pytpy proton signal. These data are given in Table 4, and are grouped according to the solvents used for the hexafluoridophosphate salts. With the exception of the pendant pyridine protons (H^{C2} and H^{C3}) in $[Ru(\mathbf{5})_2]^{4+}$, similar trends are observed for each complex in a common pair of solvents. This suggests that changing the *N*-substituent has little effect on the interaction between cation and anion, except in the case of the *N*–CH_2CN substituent (ligand **5**).

Table 4 Changes in ^1H NMR chemical shift values on going from $[RuL_2][PF_6]_4$ to $[RuL_2][HSO_4]_4$ (L^+ = **1–7**): $\Delta\delta = \delta([PF_6]^-$ salt) − $\delta([HSO_4]^-$ salt)

Δδ values							
Complex	H^{B3}	H^{C2}	H^{C3}	H^{A3}	H^{A4}	H^{A5}	H^{A6}
DMSO-d_6 for $[RuL_2][PF_6]_4$ and D_2O for $[RuL_2][HSO_4]_4$							
$[Ru(\mathbf{2})_2]^{4+}$	+0.49	+0.40	+0.33	+0.40	+0.20	+0.14	+0.15
$[Ru(\mathbf{3})_2]^{4+}$	+0.48	+0.39	+0.33	+0.39	+0.20	+0.14	+0.15
$[Ru(\mathbf{4})_2]^{4+}$	+0.51	+0.34	+0.36	+0.43	+0.21	+0.13	+0.14
$[Ru(\mathbf{5})_2]^{4+}$	+0.47	+0.25	+0.27	+0.40	+0.19	+0.12	+0.13
$[Ru(\mathbf{6})_2]^{4+}$	+0.51	+0.32	+0.35	+0.42	+0.20	+0.12	+0.13
CD_3CN for $[RuL_2][PF_6]_4$ and D_2O for $[RuL_2][HSO_4]_4$							
$[Ru(\mathbf{1})_2]^{4+}$	−0.11	−0.12	−0.04	+0.02	+0.05	+0.05	+0.01
$[Ru(\mathbf{7})_2]^{4+}$	−0.15	−0.16	−0.06	−0.01	+0.04	+0.04	+0.01

Table 5 UV-Vis spectroscopic data for aqueous solutions of $[RuL_2][HSO_4]_4$ (L^+ = **1–7**)

Complex	MLCT/nm ($\varepsilon/10^3$ dm^3 mol^{-1} cm^{-1})	Ligand-centred $\pi^*\leftarrow\pi$/nm ($\varepsilon/10^3$ dm^3 mol^{-1} cm^{-1})				
$[Ru(\mathbf{1})_2]^{4+}$	511 (37.8)	341 (34.4)	308 (30.8)	281 sh (62.2)	276 (75.4)	241 (48.2)
$[Ru(\mathbf{2})_2]^{4+}$	513 (33.7)	342 (31.8)	310 (26.1)	284 sh (58.2)	277 (67.8)	
$[Ru(\mathbf{3})_2]^{4+}$	518 (29.8)	342 (21.8)	307 sh (18.1)	285 sh (57.4)	277 (67.3)	
$[Ru(\mathbf{4})_2]^{4+}$	508 (24.6)	340 (23.9)	308 (11.4)	287 sh (36.1)	276 (50.3)	
$[Ru(\mathbf{5})_2]^{4+}$	518 (35.1)	342 (33.6)	307 (32.2)	283 sh (64.2)	277 (78.3)	238 (53.5)
$[Ru(\mathbf{6})_2]^{4+}$	511 (32.1)	340 (29.2)	309 (25.9)	288 sh (51.1)	276 (64.2)	237 (41.9)
$[Ru(\mathbf{7})_2]^{4+}$	510 (19.6)	340 (14.6)	308 (20.2)	282 sh (41.7)	276 (49.0)	

Electronic absorption and emission spectra of $[RuL_2][HSO_4]_4$

The electronic absorption spectra of aqueous solutions of $[RuL_2][HSO_4]_4$ with L^+ = **1–7** are depicted in Fig. 4. Their appearance is very similar to the absorption spectra of the hexafluoridophosphate salts in MeCN (Fig. 3), although the extinction coefficients are all lower for the hydrogensulfate salts. A comparison of Tables 1 and 5 confirms that the energies of the absorption maxima are little affected by the change of anion and solvent.

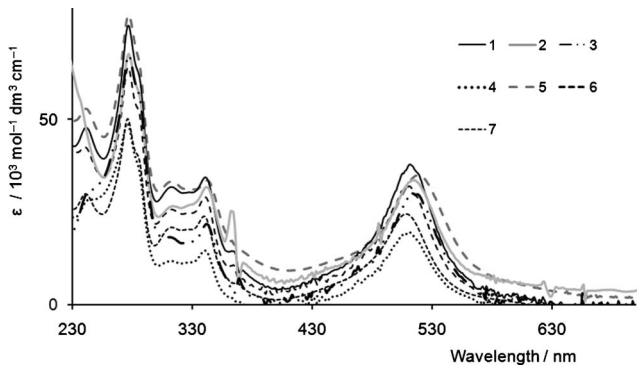

Fig. 4 Electronic absorption spectra of aqueous solutions of $[RuL_2][HSO_4]_4$ (L^+ = **1** to **7**). The absorption data are given in Table 5.

The emission properties of aqueous solutions of $[RuL_2][HSO_4]_4$ with L^+ = **1–7** are summarized in Table 6. For each complex, excitation in the MLCT band (λ_{ex} = 510 nm) produced an emission around 720–730 nm, similar to that observed for the corresponding hexafluoridophosphate salt in MeCN. There is a decrease in the emission lifetime on going from $[RuL_2][PF_6]_4$ to $[RuL_2][HSO_4]_4$ for each ligand, but the trends (longest lived emitters for *N*-ethyl, *N*-octyl and *N*-benzyl derivatives, and introduction of cyano or nitro substituents shortening the lifetime) remained the same.

DFT and TD-DFT calculations

TD-DFT is a powerful computational technique that is the method of choice for characterizing electronic transitions observed experimentally in UV-Vis absorption spectroscopy.[42–46] We have employed TD-DFT to compare calculated and experimental structural data for representative $[RuL_2]^{4+}$ complexes (L^+ = **1** and **4**), to identify the composition of the MOs involved in the MLCT transitions, and to gain insight into the effect of altering pytpy *N*-substituents on the UV-Vis absorption spectra of the series of complexes $[RuL_2]^{4+}$ with L^+ = **1–7**.

Table 6 Emission maxima, λ_{em} (λ_{ex} = 510 nm), lifetimes, τ, (475 nm laser diode) and quantum yields, Φ, for $[RuL_2][HSO_4]_4$ (L^+ = **1–7**) in aqueous solution at room temperature. For each, λ_{ex} = 510 nm

Complex	λ_{em}/nm	τ/ns	Φ (±15%)
$[Ru(\mathbf{1})_2]^{4+}$	719	135	0.0060
$[Ru(\mathbf{2})_2]^{4+}$	722	108	0.0045
$[Ru(\mathbf{3})_2]^{4+}$	724	103	0.0042
$[Ru(\mathbf{4})_2]^{4+}$	732	146	0.0062
$[Ru(\mathbf{5})_2]^{4+}$	734	98	0.0009
$[Ru(\mathbf{6})_2]^{4+}$	716	137	0.0051
$[Ru(\mathbf{7})_2]^{4+}$	722	142	0.0063

Table 7 Comparison of DFT and X-ray crystal structure geometrical parameters in the coordination sphere of the ruthenium atom in $[Ru(\mathbf{1})_2]^{4+}$ and $[Ru(\mathbf{4})_2]^{4+}$. Atom numbering corresponds to Fig. 1

Parameter	L^+ = **1** (DFT)	L^+ = **1** (expt)	L^+ = **4** (DFT)	L^+ = **4** (expt)
Ru1–N1/Å	2.129	2.064(6)	2.128	2.076(3)
Ru1–N2/Å	2.017	1.966(5)	2.015	1.981(3)
Ru1–N3/Å	2.127	2.06796)	2.128	2.088(3)
Ru1–N5/Å	2.127	2.073(5)	2.128	2.082(4)
Ru1–N6/Å	2.016	1.969(5)	2.015	1.976(3)
Ru1–N7/Å	2.129	2.080(5)	2.128	2.075(4)
N4–C21/Å	1.518	1.500(9)	1.494	1.487(19)
N8–C43/Å	1.518	1.49(1)	1.494	1.486(6)
N2–Ru1–N1/°	78.27	79.0(2)	78.33	79.37(14)
N2–Ru1–N3/°	78.24	78.1(2)	78.30	78.44(14)
N5–Ru1–N6/°	78.30	78.6(2)	78.33	78.70(14)
N6–Ru1–N7/°	78.27	79.1(2)	78.30	78.95(14)

In addition to the solid state structure of $[Ru(\mathbf{4})_2][PF_6]_4\cdot H_2O$ reported in this work, we have previously described the structure of $[Ru(\mathbf{1})_2][PF_6]_4\cdot 2(Me_2CO)\cdot 0.3$ MeCN.[14] A comparison of the data listed in Table 7 for $[Ru(\mathbf{1})_2]^{4+}$ and $[Ru(\mathbf{4})_2]^{4+}$ shows good agreement between experimental and calculated bond parameters; the DFT bond lengths are typically within 0.1 Å of single crystal X-ray data, and angles are within one degree. The root-mean-square deviations (RMSD) of the atomic coordinates of the Ru(pytpy)$_2$-cores of $[Ru(\mathbf{1})_2]^{4+}$ and $[Ru(\mathbf{4})_2]^{4+}$ when the DFT and X-ray structures are overlaid are 0.171 and 0.543 Å, respectively. The larger RMSD value for the latter appears to have its origins in ring C (Scheme 1) being slightly rotated in the calculated structure with respect to the crystallographically determined structure. The level of agreement found between DFT and crystallographic data helps to confirm that the geometries generated by the B3LYP optimizations are realistic.

Electronic transition data extracted from the TD-DFT calculations for $[RuL_2]^{4+}$ (L^+ = **1–7**) are presented in Table 8, and predict absorptions lying in the range of 480 to 505 nm. As seen in

Table 8 Wavelength λ of TD-DFT absorption signals (nm) and oscillator strength (f) for the complexes

Complex	λ_1/nm	f_1	λ_2/nm	f_2
$[Ru(pytpy)_2]^{2+}$	445.9	0.294	410.5	0.184
$[Ru(\mathbf{1})_2]^{4+}$	478.4	0.616	412.0	0.176
$[Ru(\mathbf{2})_2]^{4+}$	486.3	0.664	412.2	0.171
$[Ru(\mathbf{3})_2]^{4+}$	488.3	0.673	412.0	0.169
$[Ru(\mathbf{4})_2]^{4+}$	478.8	0.580	412.4	0.167
$[Ru(\mathbf{5})_2]^{4+}$	504.6	0.667	411.7	0.147
$[Ru(\mathbf{6})_2]^{4+}$	481.6	0.615	412.4	0.164
$[Ru(\mathbf{7})_2]^{4+}$	481.0	0.653	412.2	0.194

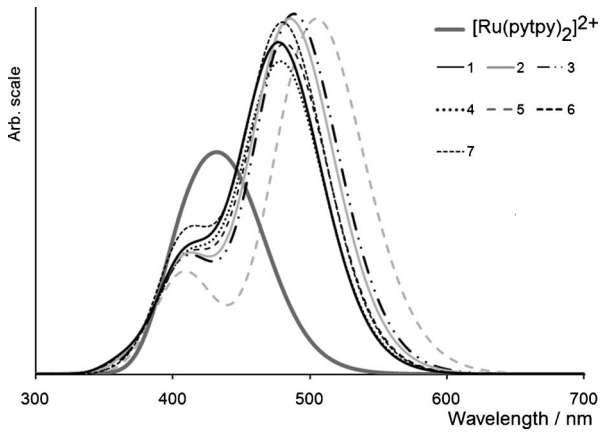

Fig. 5 TD-DFT calculated spectra of $[Ru(pytpy)_2]^{2+}$ and $[RuL_2]^{4+}$ with L^+ = **1**–**7**. Only the first fifteen transitions were examined (high energy limit ≈350 nm). The figure was generated using the GaussSum program.[31]

Fig. 5, each calculated absorption band for $[RuL_2]^{4+}$ is composed of two components which result in a main band with a higher energy shoulder. This nicely reproduces the asymmetry of the experimentally observed band (Fig. 6). For the parent complex $[Ru(pytpy)_2]^{2+}$, the calculated absorption maximum is at 431 nm. The calculated band is the sum of two components (as in the alkylated complexes) with individual λ values of 410 and 446 nm. The energy separation of these components is less than in the alkylated derivatives, and a single broad peak is visible in Fig. 5. The calculated absorption maxima for $[RuL_2]^{4+}$ are systematically blue-shifted with respect to the experimentally observed bands. The latter appear between 509 and 513 nm for $[RuL_2][PF_6]_4$ (Table 1) and between 508 and 518 nm for $[RuL_2][HSO_4]_4$ (Table 5). The difference of about 0.15 eV represents an acceptable level of agreement. It is pleasing that the calculated spectra predict: (i) a red shift in λ_{max} on going from $[Ru(pytpy)_2]^{2+}$ to $[RuL_2]^{4+}$, (ii) little variation in λ_{max} within the series of $[RuL_2]^{4+}$ complexes with L^+ = **1**–**7**, (iii) that the most red-shifted λ_{max} within the series is for $[Ru(\mathbf{5})_2]^{4+}$, and (iv) that the most blue-shifted λ_{max} is for $[Ru(\mathbf{4})_2]^{4+}$. All of these predictions replicate the experimental findings presented in Tables 1 and 5, and Fig. 3 and 4. The TD-DFT calculations correctly predict a red shift on going from $[Ru(pytpy)_2]^{2+}$ (Table 1) to $[RuL_2]^{4+}$. Overall, the agreement between TD-DFT and experimental data gives confidence that the calculations correctly identify the electronic transitions giving rise to the observed MLCT absorption maxima.

The TD-DFT calculations allow us to probe the composition of the MOs involved in the MLCT transitions. This is summarized in Fig. 7 for $[Ru(\mathbf{4})_2]^{4+}$, and in Figs. S1–S6† for the remaining complexes. The calculations are consistent with an MLCT description of the absorption observed around 510 nm in each experimental UV-Vis spectrum. This is attributed to an electronic transition from a metal-based, HOMO-1 set of orbitals (which are close in energy but non-degenerate since the complex does not possess the D_{2d} symmetry of the parent $[Ru(tpy)_2]^{2+}$) to ligand-based LUMOs (again, close in energy but non-degenerate). The latter extend over the π-system of the pytpy portion of the ligands. The HOMO-1 and HOMO possess predominantly d-orbital character, with the energy separation between the two levels being ≈0.1 eV (Fig. 7). The orbitals originate from the metal t_{2g} set (in ideal O_h symmetry). While each of the HOMO-1 orbitals lies at ≈45° to the planes of the two tpy domains (Fig. 8), the HOMO is orthogonal to both tpy units (Fig. 8) and cannot, by symmetry, contribute to the MLCT transition. The LUMO is localised on the $[Ru(pytpy)_2]$-core and does not have significant character beyond the nitrogen atom of the pendant pyridine ring (N4 and N8 in Fig. 1) of each complex. The methylene linker connecting atoms N4 and N8 to the substituents interrupts the π-system, restricting the electronic influence of the alkyl substituents on the energy of the LUMOs.

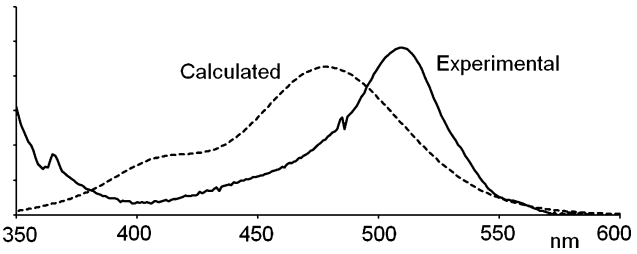

Fig. 6 Comparison of experimental and calculated electronic absorption spectra (MLCT bands) of $[Ru(\mathbf{4})_2]^{4+}$. The experimental spectrum is for the hexafluoridophosphate salt in MeCN, and has been scaled so that the peak intensities of the two spectra are comparable.

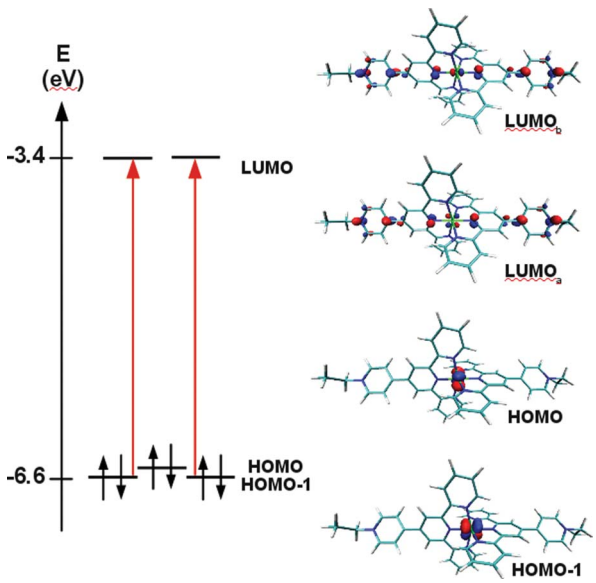

Fig. 7 Diagram showing the relative energies of the highest occupied and lowest unoccupied MOs of $[Ru(\mathbf{4})_2]^{4+}$, and transitions responsible for the MLCT absorption in the electronic spectrum. Isodensity surfaces are displayed on the right. The two HOMO-1 orbitals (shown together as the sum of two MOs) are close in energy but are non-degenerate, and similarly for the two orbitals labelled LUMO.

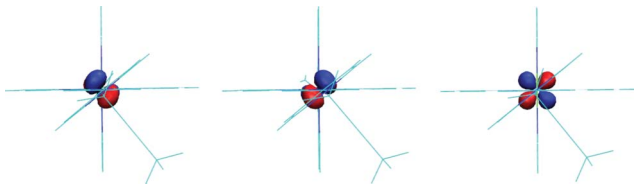

Fig. 8 The two isoenergetic HOMO-1 orbitals (left and middle) and the HOMO (right) centered on the Ru atom in $[Ru(\mathbf{4})_2]^{4+}$. The view is along the $N_{py} \cdots Ru \cdots N_{py}$ axis, showing one tpy group lying in the horizontal plane and the other tpy group lying perpendicular. In the foreground at roughly 45° to both tpy groups is one pendant pyridine ring, and perpendicular to that is the ethyl substituent.

Conclusions

Starting from $[Ru(pytpy)_2][PF_6]_2$, we have synthesized a series of *N*-alkylated derivatives $[RuL_2][PF_6]_4$ in which $L^+ = \mathbf{2}$–$\mathbf{7}$ (Scheme 1), and have reported their solution NMR spectroscopic, electrochemical and photophysical properties. The crystal structure of $[Ru(\mathbf{4})_2][PF_6]_4 \cdot H_2O$ confirmed *N*-alkylation on both pendant pyridine rings. For their application as photosensitizers in water oxidation, it is advantageous that water soluble salts be prepared. Thus, $[RuL_2][HSO_4]_4$ complexes ($L^+ = \mathbf{1}$–$\mathbf{7}$) have been synthesized by anion exchange from $[RuL_2][PF_6]_4$. With the exception of $[Ru(\mathbf{5})_2]^{4+}$, changing the anion and solvent has similar effects on the chemical shifts of the resonances in the ^1H NMR spectra for each complex, suggesting that altering the *N*-substituent has negligible influence on the cation–anion interactions except in the case of the substituent being *N*–CH_2CN. Going from the hexafluoridophosphate to hydrogensulfate salts has little effect on the energies of absorptions in the electronic spectra, but a decrease in extinction coefficients is observed for all the complexes. The emission spectra and lifetimes for the hexafluoridophosphate and hydrogensulfate salts show parallel trends. All exhibit an emission around 720–730 nm (λ_{ex} = 510 nm). For each ligand, the emission lifetime decreases on going from $[RuL_2][PF_6]_4$ to $[RuL_2][HSO_4]_4$, but the trends (longest lived emitters for *N*-ethyl, *N*-octyl and *N*-benzyl derivatives, and shortest lived emitters for cyano or nitro derivatives) were the same for both salts.

A complementary theoretical study has shown a satisfactory level of agreement between DFT and crystallographic data for $[Ru(\mathbf{1})_2]^{4+}$ and $[Ru(\mathbf{4})_2]^{4+}$. Calculated (TD-DFT) absorption spectra predict a red shift in λ_{max} on going from $[Ru(pytpy)_2]^{2+}$ to $[RuL_2]^{4+}$, and minor variations in λ_{max} within the series of $[RuL_2]^{4+}$ complexes ($L^+ = \mathbf{1}$–$\mathbf{7}$). The theoretical data predict that the most red-shifted λ_{max} occurs for $[Ru(\mathbf{5})_2]^{4+}$, and the most blue-shifted is for $[Ru(\mathbf{4})_2]^{4+}$. These results are in keeping with experimental observations. Analysis of the compositions of the MOs involved in the MLCT transitions confirms that there is no contribution from orbitals on the *N*-alkyl substituents, thereby supporting the fact that varying the pytpy *N*-substituents has little effect on the energy of the MLCT band.

Acknowledgements

We thank the Swiss National Science Foundation and the University of Basel for financial support. M. Devereux wishes to thank Dr Nohad Gresh for access to computing resources and for helpful feedback. The computations reported in this work were performed using resources from GENCI (CINES/IDRIS), grant 2009-075009 and grant x2010075027. Lukas Jundt is acknowledged for preliminary results. We acknowledge the assistance of Ewald Schönhofer with TGA measurements.

Notes and references

1 E. C. Constable, *Adv. Inorg. Chem.*, 1986, **30**, 69.
2 R. P. Thummel, in *Comprehensive Coordination Chemistry II*, ed. J. A. McCleverty and T. J. Meyer, Elsevier, 2004, vol. 1, p. 41.
3 H. Hofmeier and U. S. Schubert, *Chem. Soc. Rev.*, 2004, **33**, 373.
4 U. S. Schubert, G. Hochwimmer and M. Heller, *ACS Symposium Series*, 2002, **812**, 163.
5 E. C. Constable, *Coord. Chem. Rev.*, 2008, **252**, 842.
6 J.-P. Sauvage, J.-P. Collin, J.-C. Chambron, S. Guillerez and C. Coudret, *Chem. Rev.*, 1994, **94**, 993.
7 E. C. Constable and A. M. W. Cargill Thompson, *J. Chem. Soc., Dalton Trans.*, 1992, 2947.
8 E. C. Constable and A. M. W. Cargill Thompson, *J. Chem. Soc., Dalton Trans.*, 1994, 1409.
9 E. C. Constable, C. E. Housecroft, M. Neuburger, D. Phillips, P. R. Raithby, E. Schofield, E. Sparr, D. A. Tocher, M. Zehnder and Y. Zimmermann, *J. Chem. Soc., Dalton Trans.*, 2000, 2219.
10 J. E. Beves, E. L. Dunphy, E. C. Constable, C. E. Housecroft, C. J. Kepert, M. Neuburger, D. J. Price and S. Schaffner, *Dalton Trans.*, 2008, 386.
11 E. C. Constable, C. E. Housecroft, A. Cargill Thompson, P. Passaniti, S. Silvi, M. Maestri and A. Credi, *Inorg. Chim. Acta*, 2007, **360**, 1102.
12 S. Silvi, E. C. Constable, C. E. Housecroft, J. E. Beves, E. L. Dunphy, M. Tomasulo, F. M. Raymo and A. Credi, *Chem.–Eur. J.*, 2008, **15**, 178.
13 S. Silvi, E. C. Constable, C. E. Housecroft, J. E. Beves, E. L. Dunphy, M. Tomasulo, F. M. Raymo and A. Credi, *Chem. Commun.*, 2009, 1484.
14 E. C. Constable, E. L. Dunphy, C. E. Housecroft, W. Kylberg, M. Neuburger, S. Schaffner, E. R. Schofield and C. B. Smith, *Chem.–Eur. J.*, 2006, **12**, 4600.
15 A. L. Kaledin, Z. Huang, Q. Yin, E. L. Dunphy, E. C. Constable, C. E. Housecroft, Y. V. Geletii, T. Lian, C. L. Hill and D. G. Musaev, *J. Phys. Chem. A*, 2010, **114**, 6284.
16 *Stoe & Cie, IPDS software v. 1.26*, Stoe & Cie, Darmstadt, Germany, 1996.
17 G. M. Sheldrick, *Acta Crystallogr., Sect. A: Found. Crystallogr.*, 2008, **64**, 112.
18 L. J. Farrugia, *J. Appl. Crystallogr.*, 1997, **30**, 565.
19 I. J. Bruno, J. C. Cole, P. R. Edgington, M. K. Kessler, C. F. Macrae, P. McCabe, J. Pearson and R. Taylor, *Acta Crystallogr., Sect. B: Struct. Sci.*, 2002, **58**, 389.
20 C. F. Macrae, I. J. Bruno, J. A. Chisholm, P. R. Edgington, P. McCabe, E. Pidcock, L. Rodriguez-Monge, R. Taylor, J. van de Streek and P. A. Wood, *J. Appl. Crystallogr.*, 2008, **41**, 466.
21 M. J. Frisch, G. W. Trucks, H. B. Schlegel, G. E. Scuseria, M. A. Robb, J. R. Cheeseman, G. Scalmani, V. Barone, B. Mennucci, G. A. Petersson, H. Nakatsuji, M. Caricato, H. P. Hratchian, A. F. Izmaylov, J. Bloino, G. Zheng, J. L. Sonnenberg, M. Hada, M. Ehara, K. Toyota, R. Fukuda, J. Hasegawa, M. Ishida, T. Nakajima, Y. Honda, O. Kitao, H. Nakai, T. Vreven, J. A. Montgomery Jr, J. E. Peralta, F. Ogliaro, M. Bearpark, J. J. Heyd, E. Brothers, K. N. Kudin, V. N. Staroverov, R. Kobayashi, J. Normand, K. Raghavachari, A. Rendell, J. C. Burant, S. S. Iyengar, J. Tomasi, M. Cossi, N. Rega, J. M. Millam, M. Klene, X. Li, J. E. Knox, J. B. Cross, V. Bakken, C. Adamo, J. Jaramillo, R. Gomperts, R. E. Startmann, O. Yazyev, A. J. Austin, R. Cammi, C. Pomelli, J. W. Ochterski, R. L. Martin, K. Morokuma, V. G. Zakrzewski, G. A. Voth, P. Salvador, J. J. Dannenberg, J. M. Dapprich, A. D. Daniels, Ö. Farkas, J. B. Foresman, J. V. Ortiz, J. Cioslowski and D. J. Fox, *Gaussian 09, Revision A.1*, Gaussian, Inc., Wallingford, CT, 2009.
22 P. J. Hay and W. R. Wadt, *J. Chem. Phys.*, 1985, **82**, 270.
23 K. L. Schuchardt, B. T. Didier, T. Elsethagen, L. Sun, V. Gurumoorthi, J. Chase, J. Li and T. L. Windus, *J. Chem. Inf. Model.*, 2007, **47**, 1045.
24 A. D. Becke, *J. Chem. Phys.*, 1993, **98**, 5648; C. Lee, R. Yang and W. G. Parr, *Phys. Rev. B*, 1988, **37**, 785.

25 M. T. Cancès, B. Mennucci and J. Tomasi, *J. Chem. Phys.*, 1997, **107**, 3032.
26 B. Mennucci and J. Tomasi, *J. Chem. Phys.*, 1997, **106**, 5151.
27 B. Mennucci, E. Cancès and J. Tomasi, *J. Phys. Chem. B*, 1997, **101**, 10506.
28 J. Tomasi, B. Mennucci and E. Cancès, *THEOCHEM*, 1999, **464**, 211.
29 K. C. D. Robson, B. D. Koivisto, T. J. Gordon, T. Baumgartner and C. P. Berlinguette, *Inorg. Chem.*, 2010, **49**, 5335.
30 Y. Yang, M. N. Weaver and K. M. Merz Jr., *J. Phys. Chem. A*, 2009, **113**, 9843.
31 N. M. O'Boyle, A. L. Tenderholt and K. M. Langner, *J. Comput. Chem.*, 2008, **29**, 839.
32 W. Humphrey, A. Dalke and K. Schulten, *J. Mol. Graphics*, 1996, **14**, 33.
33 J. E. Beves, D. J. Bray, J. K. Clegg, E. C. Constable, C. E. Housecroft, K. A. Jolliffe, C. J. Kepert, L. F. Lindoy, M. Neuburger, D. J. Price, S. Schaffner and F. Schaper, *Inorg. Chim. Acta*, 2008, **361**, 2582.
34 J. E. Beves, E. L. Dunphy, E. C. Constable, C. E. Housecroft, C. J. Kepert, M. Neuburger, D. J. Price and S. Schaffner, *Dalton Trans.*, 2008, 386.
35 E. C. Constable, C. E. Housecroft, E. A. Medlycott, M. Neuburger, F. Reinders, S. Reymann and S. Schaffner, *Inorg. Chem. Commun.*, 2008, **11**, 805.
36 E. C. Constable, C. E. Housecroft, M. Neuburger, S. Schaffner and F. Schaper, *Inorg. Chem. Commun.*, 2006, **9**, 616.
37 J. McMurtrie and I. Dance, *CrystEngComm*, 2010, **12**, 3207.
38 J. McMurtrie and I. Dance, *CrystEngComm*, 2009, **11**, 1141.
39 J. E. Beves, P. Chwalisz, E. C. Constable, C. E. Housecroft, M. Neuburger, S. Schaffner and J. A. Zampese, *Inorg. Chem. Commun.*, 2008, **11**, 1009.
40 E. C. Constable, C. E. Housecroft, E. A. Medlycott, M. Neuburger, F. Reinders, S. Reymann and S. Schaffner, *Inorg. Chem. Commun.*, 2008, **11**, 805.
41 R. K. Harris, E. D. Becker, S. M. Cabral de Menezes, R. Goodfellow and P. Granger, *Pure Appl. Chem.*, 2001, **73**, 1795.
42 S. Fantacci, F. De Angelis and A. Selloni, *J. Am. Chem. Soc.*, 2003, **125**, 4381.
43 C. Barolo, Md. K. Nazeeruddin, S. Fantacci, D. Di Censo, P. Comte, P. Liska, G. Viscardi, P. Quagliotto, F. De Angelis, S. Ito and M. Grätzel, *Inorg. Chem.*, 2006, **45**, 4642.
44 K. C. D. Robson, B. D. Koivisto, T. J. Gordon, T. Baumgartner and C. P. Berlinguette, *Inorg. Chem.*, 2010, **49**, 5335.
45 Md. K. Nazeeruddin, T. Bessho, L. Cevey, S. Ito, C. Klein, F. De Angelis, S. Fantacci, P. Comte, P. Liska, H. Imai and M. Grätzel, *J. Photochem. Photobiol., A*, 2007, **185**, 331.
46 I. Ciofini Ilaria, P. P. Lainé, F. Bedioui and C. Adamo, *J. Am. Chem. Soc.*, 2004, **126**, 10763.